

## A Pre-Protostellar Core in L1551. II. State of Dynamical and Chemical Evolution

Jonathan J. Swift<sup>1</sup> and William J. Welch

*Department of Astronomy and Radio Astronomy Laboratory, University of California, 601 Campbell Hall, Berkeley, CA 94720-3411*

James Di Francesco

*National Research Council of Canada, Herzberg Institute of Astrophysics, 5071 West Saanich Road, Victoria, BC V9E 2E7, Canada*

Irena Stojimirović

*Department of Astronomy, University of Massachusetts, LGRT-B 619E, 710 North Pleasant St., Amherst, MA 01003-9305*

### ABSTRACT

Both analytic and numerical radiative transfer models applied to high spectral resolution CS and N<sub>2</sub>H<sup>+</sup> data give insight into the evolutionary state of L1551 MC. This recently discovered pre-protostellar core in L1551 appears to be in the early stages of dynamical evolution. Line-of-sight infall velocities of  $\gtrsim 0.1 \text{ km s}^{-1}$  are needed in the outer regions of L1551 MC to adequately fit the data. This translates to an accretion rate of  $\sim 10^{-6} M_{\odot} \text{ yr}^{-1}$ , uncertain to within a factor of 5 owing to unknown geometry. The observed dynamics are not due to spherically symmetric gravitational collapse and are not consistent with the standard model of low-mass star formation. The widespread, fairly uniform CS line asymmetries are more consistent with planar infall. There is modest evidence for chemical depletion in the radial profiles of CS and C<sup>18</sup>O suggesting that L1551 MC is also chemically young. The models are not very sensitive to chemical evolution. L1551 MC lies within a quiescent region of L1551 and is evidence for continued star formation in this evolved cloud.

*Subject headings:* ISM: clouds — ISM: individual(L1551) — stars: formation — line: profiles — radiative transfer

---

<sup>1</sup>js@astro.berkeley.edu

## 1. Introduction

Gravitationally bound molecular cores with no embedded infrared sources, referred to as pre-protostellar cores (PPCs), offer the unique opportunity to study the conditions preceding stellar birth. To date there have only been a few PPCs studied in depth leaving many unanswered questions regarding the kinematics and chemistry during this epoch of star formation.

Inward gas motions are necessary for the formation of stars and the kinematic signatures of these motions are expected to be present in molecular line data. Blue-peaked asymmetric line profiles commonly seen in optically thick tracers of molecular cores can be accurately modeled as self-absorbed infalling gas (Evans 1999; Myers et al. 1996). A high ratio of blue-peaked to red-peaked profiles in selected cores is further evidence that these spectral signatures are tracing global infall in some PPCs (Lee et al. 2001). These “infall asymmetries” imply infall velocities of up to  $\sim 0.1 \text{ km s}^{-1}$  extending out to  $\sim 0.1 \text{ pc}$  (Tafalla et al. 1998; Lee et al. 2001) inconsistent with the ambipolar diffusion paradigm of isolated low-mass star formation (Shu, Adams & Lizano 1987; Ciolek & Mouschovias 1995).

The observed decrement in abundance of certain molecules such as CO and CS toward the centers of cores (Kuiper et al. 1996; Willacy et al. 1998; Caselli et al. 1999; Tafalla et al. 2002) can be explained by the expected depletion of these species onto dust grains (Watson & Salpeter 1972; Bergin & Langer 1997). In some PPCs the abundance profile is best fit using a model with a central region of complete depletion (e.g., Tafalla et al. 2004). Models have shown that depletion becomes more severe as a core collapses suggesting that chemical depletion may be useful in determining the age of PPCs (Rawlings et al. 1992; Bergin & Langer 1997; Lee et al. 2004; Aikawa et al. 2005). However, detailed molecular line studies have shown that chemistry is not reliable as a sole evolutionary indicator (Lee et al. 2003) and interpretations should be made on a case by case basis (Rawlings & Yates 2001).

Analytic models of asymmetric molecular line profiles (e.g. Myers et al. 1996) provide quick solutions by imposing functional forms for molecular excitation and chemistry along the line of sight. These models have been shown to reliably characterize simulated data despite using the simplest available assumptions (De Vries & Myers 2005). Numerical models typically contain less assumptions and are hence more flexible, but are computationally much more costly.

L1551 MC is a PPC that sits in a relatively isolated region to the northwest of IRS5 in the well-known L1551 dark cloud (Swift et al. 2005, hereafter Paper I). It is expected to be gravitationally unstable and hints of infall have been seen in position switched CS spectra. The differentiation seen between the  $\text{NH}_3$  and  $\text{C}_2\text{S}$  emission suggests chemical evolution.

Past studies of the L1551 cloud (e.g., Snell 1981; Devine, Reipurth & Bally 1999) provide a well-defined context for L1551 MC. Following the discovery and primary characterization of this starless molecular core (Paper I), this article investigates dynamical and chemical signatures from new molecular line data in an attempt to understand its state of evolution toward stellar birth.

In §2 we outline the molecular line observations used with the observations of Paper I to analyze L1551 MC. The models used to interpret these data are described in §3 with the results presented in §4. Further consideration of these results in §5 reveal the main conclusions of this paper which are then summarized in §6.

## 2. Observations and Reductions

We used the Five College Radio Astronomy Observatory’s 14 m telescope on the nights of 2005 January 7 and 8, and for partial nights on February 8, 9 and 24 to map L1551 MC in  $\text{N}_2\text{H}^+$  and CS simultaneously. The weather was variable on the nights of January 7 and 8 with system temperatures varying from  $\sim 220$  K to  $\sim 375$  K. The partial nights were substantially better showing system temperatures from 130 K to 150 K.

The observing frequencies in the first and second IF of the dual channel correlator (DCC) were set to 93.176258 GHz and 97.980953 GHz, corresponding to the isolated component of the  $\text{N}_2\text{H}^+(1-0)$  and the  $\text{CS}(2-1)$  rotational transitions (Lee et al. 2001) respectively, for our maps. The beam at these observing frequencies has a FWHM of  $\sim 45''$  and a main beam efficiency  $\eta_b \approx 0.5$ . The highest spectral resolution mode of the DCC was used giving a 25 MHz band with 1024 channels resulting in  $\sim 0.08$  km s $^{-1}$  velocity resolution.

A  $6' \times 6'$  patch of sky was mapped centered on L1551 MC,  $4^{\text{h}}31^{\text{m}}09^{\text{s}}.9$ ,  $+18^{\circ}12'41''$  (J2000.0), using the on-the-fly observing technique. Our final maps are a composite of  $\sim 20$  individual maps created by scanning alternatively in the right ascension and declination directions combined by weighted mean. These maps are highly oversampled given the  $12''$  row spacing,  $60''$  s $^{-1}$  scan speed and the rotation of the SEQUOIA 32 element receiver array with parallactic angle. The data are calibrated with an OFF scan every two rows and a total power calibration scan every four rows. These data were reduced, gridded and output to FITS files using the OTFTOOL utility available at the observatory. The RMS noise level in our final CS and  $\text{N}_2\text{H}^+$  maps is  $\sim 26$  mK. All further analysis was performed using the IDL software of Research Systems Inc.

### 3. Models

We use a non-linear least squares minimization based on the Levenberg-Marquardt technique to find the best fits to our spectral line data according to two distinctly different radiative transfer models. The analytic model fits the asymmetric CS line profiles while the family of numerical models use information from the optically thin  $\text{N}_2\text{H}^+$  emission to fit both the CS and the CO isotopologue data.

#### 3.1. Analytical Model

The HILL5 model presented in De Vries & Myers (2005) assumes a symmetric 1-dimensional structure for all parameters. The central excitation temperature,  $T_C$ , tapers linearly to the cloud edge where it has a value of  $T_b = 2.73$  K. Gas approaches the center of this model system at a constant velocity,  $v_{in}$ , relative to the systemic velocity,  $v_{LSR}$ . Including the central optical depth,  $\tau_C$ , and the velocity dispersion of the gas,  $\sigma$ , there are a total of 5 free parameters. The HILL5 model is the preferred model in De Vries & Myers (2005) giving estimates of the infall velocity in simulated observations good to  $0.02 \text{ km s}^{-1}$ .

#### 3.2. Numerical Models

The “RT” program introduced in Dickel & Auer (1994) (also see Williams et al. 2004) computes the full, non-equilibrium radiative transfer for a spherically symmetric mass. This FORTRAN code takes the density, kinematics, kinetic temperature and molecular abundance ratio as a function of core radius and solves for the level populations using a lambda-iteration technique.

Table 1 outlines the fixed and free parameters which define our family of numerical models and Table 2 summarizes the individual models described in the following subsections. The density of molecular hydrogen is represented by  $n$ . The density of a molecular species is denoted by  $n_{mol}$  and is related to the total density by the conversion factor,  $X_{mol}$ . The infall velocity,  $v_{in}$ , is equal to  $v_0$  at the minimum radius of the model and follows a power law form with index  $p$ . The model core is isothermal with a constant turbulent velocity width  $\Delta v_{turb}$ . Quantities are evaluated at 40 logarithmically spaced radii from  $r_{min}$  to  $r_{max}$ . The fixed parameters, except for the radii, are derived from the  $\text{NH}_3$  data of Paper I. The maximum radius represents the extent of the CS emission. The minimum radius was chosen in consideration of a timely convergence and our results are not sensitive to its exact value. All models have as free parameters  $n_0$ ,  $v_0$ , and  $X_{mol}$ .

Each numerical model comprises a substantial parameter space to explore. The density and infall velocities are therefore constrained to  $10^3 < n_0 < 10^7 \text{ cm}^{-3}$  and  $0 < v_{in} < 0.5 \text{ km s}^{-1}$  in accord with the results of Paper I. For each model the best fit was determined by repeating the least-squares minimization procedure beginning at randomly chosen parameter values until the global minimum in  $\chi^2$  space was converged upon.

These models were first used to fit the CS(2 – 1) line profiles and then modified to fit for the conversion factors for  $^{13}\text{CO}$  and  $\text{C}^{18}\text{O}$  given the best fit parameters from the CS fits. The kinetic temperature and turbulent velocity width are also free parameters in these fits to account for the possibility that the CO isotopologues are tracing different environments within L1551 MC. Upper limits of 12 K (Snell 1981) and  $0.5 \text{ km s}^{-1}$  were enforced for  $T_K$  and  $\Delta v_{turb}$  respectively.

The systemic velocity for all the numerical models is obtained from fits to the full  $\text{N}_2\text{H}^+(1 - 0)$  transition with the hyperfine fitting routine developed in Paper I. This routine returns the optical depth, velocity centroid, velocity width, and excitation temperature for a given spectrum.

The normalized root mean square of the error is used as our goodness of fit indicator defined by

$$RMSE = \frac{1}{\sigma} \sqrt{\frac{1}{N} \sum_{i=1}^N (y_i - \hat{y}_i)^2} \quad (1)$$

where  $\sigma$  is the RMS noise level in the spectrum,  $N$  is the number of data points used in the fit,  $y_i$  are the data points and  $\hat{y}_i$  are the model points. Values of  $RMSE \sim 1$  are expected for successful fits.

There are six total numerical models denoted by an identifier and a Roman numeral (Table 2). Each pair of models are identical except for the abundance profile which is either constant throughout or takes the form

$$X_{mol} = \begin{cases} 0 & : r_{min} \leq r \leq r_c \\ \text{constant} & : r_c < r \leq r_{max} \end{cases} \quad (2)$$

which is referred to as a “drop” abundance profile. The models are further grouped by the assumed velocity structure into two main categories, accretion and collapse.

### 3.2.1. “Accretion” Models

The first four models are referred to as “accretion” models because they allow for the possibility of high velocity gas in the outer regions of the core. Model ACV-I is like the HILL5 analytic model, but the radiative transfer is solved for numerically. Therefore, the infall velocity from ACV-I can be compared to the results of the HILL5 model for consistency. Model ACV-II is used to test whether or not having a depletion zone significantly alters the derived infall velocity.

Models A-I and II have a velocity profile that increases as the square root of the core radius and represent scenarios in which gas is accreting onto the core from large radii. These models, in comparison with the others, test if the highest velocity infalling gas is in the exterior regions of the core.

### 3.2.2. “Collapse” Models

Models GC-I and II have velocity structures chosen to represent inside-out collapse, as in Shu (1977). Given the complexity of L1551 MC from observations a detailed comparison with theoretical models would be difficult. However, free-fall collapse is generally expected to produce a decreasing velocity profile with radius from the center of the core to the rarefaction front (e.g., Fatuzzo et al. 2004; Myers 2005). Therefore these models test if the motions implied by the CS emission are consistent with the motions expected from gravitational collapse directly associated with the formation of a protostar.

## 4. Results

Figure 1 shows the distribution of velocity integrated  $\text{N}_2\text{H}^+$  in greyscale overlaid with independent CS(2–1) spectra at their respective plane-of-sky locations. The vertical dotted lines shown in selected spectra are the systemic velocities from the hyperfine fits to the  $\text{N}_2\text{H}^+$  profiles. Most CS line profiles are asymmetric having a peak blueward of the systemic velocity and a smaller red peak or shoulder.

### 4.1. Statistics of the CS Line Asymmetry

The normalized velocity difference introduced in Mardones et al. (1997) is a useful quantity to characterize spectral asymmetries. Using CS and  $\text{N}_2\text{H}^+$  as optically thick and

thin molecular species, we define

$$\delta V_{CS} = \frac{V_{CS} - V_{N_2H^+}}{\Delta V_{N_2H^+}} \quad (3)$$

where  $V_{CS}$  is the velocity centroid of the brightest peak in the CS line profile and the velocity centroid and intrinsic FWHM of the  $N_2H^+$  emission,  $V_{N_2H^+}$  and  $\Delta V_{N_2H^+}$ , are obtained from hyperfine fitting.

The  $N_2H^+$  emission is less extended than the CS emission, so it is the 31 beam-sampled spectra with well-determined centroids ( $\sigma_{V_{cen}} < 0.1\Delta V_{N_2H^+}$ ) that define our sample. Figure 2 shows a histogram of the  $\delta V_{CS}$  values. The cross-hatched area corresponds to  $\delta V_{CS}$  values that are greater than 5 times the estimated error ( $\sigma_\delta$ ) obtained from standard propagation of error. The values for  $\sigma_\delta$  range from 0.03 to 0.4 with a median of 0.10. The mean value  $\langle \delta V_{CS} \rangle = -0.50$ .

The blue excess is defined as  $E = (N_- - N_+)/N$  (Lee et al. 2001), where  $N_-$  is the number of positions with  $\delta V_{CS} \leq -5\sigma_\delta$ ,  $N_+$  is the number of positions with  $\delta V_{CS} \geq 5\sigma_\delta$  and here  $N = 31$ . The blue excess of L1551 MC is high,  $E = 0.39$ , meaning a significant fraction of CS lines have a blue peak.

The  $P$  value of the student t-test measures of the probability that a given sample of values was drawn from a normal distribution with a mean of zero. For the 31  $\delta V_{CS}$  values in L1551 MC,  $P$  is less than 0.5%. Together with a high  $E$  value, this means that the asymmetric CS profiles are not random but are strongly biased toward having a blue peak. In relation to the cores studied in Lee et al. (2001), L1551 MC would rank as a bona fide infall candidate.

## 4.2. Model Fits

The 18 spectra with  $|\delta V_{CS}| \geq 5\sigma_\delta$  are fit according to the HILL5 model. Three of these 18 spectra return positive (outflowing) gas velocities and correspond precisely to the three spectra that show positive  $\delta V_{CS}$  values in Figure 2. Of the 15 spectra that show negative (infalling) gas velocities, the mean  $\langle v_{in} \rangle = 0.13 \text{ km s}^{-1}$ , roughly two thirds the sound speed in the medium.

Averages of our molecular line data within the central  $100''$  of L1551 MC (dashed circle in Figure 1) yield high signal-to-noise composite spectra in CS,  $N_2H^+$ ,  $^{13}\text{CO}$ , and  $\text{C}^{18}\text{O}$ . The best fit to the CS composite spectrum using the HILL5 model is outlined in Table 3 and is presented as the dotted line on the CS spectrum of Figure 3. The fit is good overall, but slightly overestimates the emission in the red wing of the profile.

The results from the numerical fits are summarized in Table 4. The best fit to the CS composite spectrum was achieved with model A-II with an RMSE value of 0.77 and is shown as the dashed line on the CS spectrum of Figure 3. The constant velocity models, ACV-I and II fit the data fairly well and are in agreement with the HILL5 results, while the collapse models, GC-I and II, produce the worst agreement with the data.

## 5. Discussion

### 5.1. Dynamics

There is a surplus of blue peaked asymmetric CS line profiles in L1551 MC successfully modeled as self-absorption from globally infalling gas (§4). In both our analytic and numerical models, gas velocities  $\gtrsim 0.1 \text{ km s}^{-1}$  are needed to account for the observed CS profiles. These motions are not associated with any of the known outflows in the L1551 cloud, including those from IRS5 (Snell, Loren & Plambeck 1980; Moriarty-Schieven & Snell 1988; Moriarty-Schieven & Wannier 1991), L1551 NE (Pound & Bally 1991; Moriarty-Schieven et al. 1995; Devine, Reipurth & Bally 1999) and XZ/HL Tau (Welch et al. 2000). A closer look at our results reveals insights into the nature of these observed dynamics.

#### 5.1.1. “Collapse” vs. “Accretion”

Figure 4 shows a direct comparison between the best “collapse” model fit, GC-I, and the best “accretion” model fit, A-II. The GC models produce the least consistent fits to our data. In these models the absorbing gas is in the outer regions of the core where the excitation temperatures are lowest and where gas is moving at relatively slow velocities. Therefore, these models produce centralized self-absorption with a double peaked profile instead of the observed red shoulder. Higher values of  $v_0$  push the absorption feature slightly further to the red and this is why the best fits for the gravitational collapse models are pegged against the  $v_0 = 0.5 \text{ km s}^{-1}$  limit set by our constraint on highly supersonic gas (§3.2).

The constant velocity accretion models, ACV-I and II, do substantially better than the inside-out collapse models allowing for absorption and emission of high velocity gas. But the monotonically increasing infall velocity of the A-I and II accretion models works together with the decreasing CS excitation temperature as a function of radius to carve a smooth red shoulder in the line profile most consistent with our data. A marginally better fit to the data is achieved with the drop abundance profile of A-II and we use this as the preferred model.



### 5.1.2. High Velocity Gas at Large Core Radii

The observed self-absorption in the CS line profiles forces our numerical model fits into the optically thick regime. It is therefore the dynamics, rather than the chemistry or mass distribution, that most significantly affects the emergent line profiles. Our fits show that infalling gas is needed in the outer regions of the core to reproduce the observed CS line profiles. The HILL5 model fits to the ensemble of CS spectra also show high infall velocities at large projected core radii (see §5.1.3).

According to the standard model of low-mass star formation (Shu, Adams & Lizano 1987), a core collapses via ambipolar diffusion until it becomes supercritical and then undergoes an inside-out collapse. The high infall velocities at large core radii indicated by our models are comparable to other closely studied cores where the dynamics were found to be inconsistent with the standard model (e.g. Tafalla et al. 1998; Lee et al. 2001). From our models it is clear that the gas motions observed across L1551 MC do not represent infalling gas due to gravitational collapse and have magnitudes too large to be associated with ambipolar diffusion.

The high infall velocities observed over a large angular extent around L1551 MC are more consistent with planar accretion. Planar accretion would produce this observational signature for a wide range of inclination angles. The magnetic field around L1551 has been measured to be fairly uniform (Vrba, Strom, & Strom 1976) and a roughly constant field could facilitate a planar accretion scenario. However, measurements of the magnetic field geometry in L1551 MC are essential to clarify this situation.

From the analytic and numerical modeling of  $\text{N}_2\text{H}^+$  and CS spectra in L1551 MC it appears that gas is falling toward the mid-plane of the core from large radii. The observed dynamics are not directly related to the formation of a star, but do not preclude gravitational collapse scenarios (e.g., Fatuzzo et al. 2004).

### 5.1.3. Mass Accretion

High infall velocities are derived from the HILL5 model for a vast majority of the CS spectra which span  $\sim 6'$ , or 0.24 pc at the distance of Taurus. This loosely defines a radius at which material is infalling,  $R_{in} \sim 0.1$  pc.

The mass infall rate is estimated as the amount of material passing through a spherical surface with radius  $R_{in}$ ,  $\dot{M}_{in} = 4\pi R_{in}^2 \rho v_{in}$ . Here we use a density of  $1.2 \times 10^4 \text{ cm}^{-3}$  and an infall velocity of  $0.02 \text{ km s}^{-1}$  derived from the model A-II best fit parameters and the

density and velocity relations from Table 1 evaluated at  $R_{in}$ . The derived infall rate  $\dot{M}_{in} \sim 10^{-6} M_{\odot} \text{ yr}^{-1}$ . Values of the average density (Paper I) and average infall velocity (§ 4.2) yield an accretion rate of the same order of magnitude as does planar infall at a constant velocity of  $0.1 \text{ km s}^{-1}$ . Due to the unknown geometry and symmetry in this problem the accretion rate cannot be constrained within a factor of  $\sim 5$ .

## 5.2. Chemical Structure

### 5.2.1. Comparisons of Molecular Species

A fit to the mean spectrum within a half power contour of the  $\text{N}_2\text{H}^+$  velocity integrated emission gives a central velocity of  $6.71 \text{ km s}^{-1}$ , an observed line width of  $0.28 \text{ km s}^{-1}$  translating into a non-thermal width of  $0.25 \text{ km s}^{-1}$  for a kinetic temperature of 9 K and a total optical depth of 4.03 ( $\tau = 0.4$  for the isolated component). This is very similar to the  $\text{NH}_3$  emission with  $v_{LSR} = 6.72 \text{ km s}^{-1}$  and  $\Delta v_{nt} = 0.2 \text{ km s}^{-1}$  (Paper I). The sky distribution of  $\text{N}_2\text{H}^+$  also follows the  $\text{NH}_3$  closely with a major and minor FWHM of  $2'.9$  and  $1'.3$  oriented at a position angle of  $139^\circ$  compared to the  $\text{NH}_3$  values of  $2'.3$ ,  $1'.1$  and  $133^\circ$ . The emission from both molecular species peak at the same sky coordinates and coincide precisely with a peak in the sub-mm dust continuum (Schieven 2004). The  $\text{N}_2\text{H}^+$  velocity gradient across the core is  $1.3 \text{ km s}^{-1} \text{ pc}^{-1}$  at a position angle of  $227^\circ$  compared to the  $\text{NH}_3$  values of  $1.2 \text{ km s}^{-1} \text{ pc}^{-1}$  and  $224^\circ$ . Therefore it seems the  $\text{N}_2\text{H}^+$  and  $\text{NH}_3$  emission trace the same high-density interior gas in L1551 MC.

Figure 5 compares the radial profiles of  $\text{NH}_3$ ,  $\text{N}_2\text{H}^+$ , CS, and  $\text{C}^{18}\text{O}$ . The  $\text{NH}_3$  and  $\text{N}_2\text{H}^+$  profiles are fit using Equation 1 and the CS and  $\text{C}^{18}\text{O}$  profiles are fit using Equation 2 of Paper I. The radial distribution of  $\text{N}_2\text{H}^+$  is slightly flatter than the  $\text{NH}_3$  which may be due to a slight overabundance of  $\text{NH}_3$  in the innermost regions as seen in other Taurus cores (e.g. Tafalla et al. 2004). The CS and  $\text{C}^{18}\text{O}$  profiles are significantly flatter than the  $\text{NH}_3$  and  $\text{N}_2\text{H}^+$  suggesting that the relative abundance of these species is higher at larger radii. While this may be due in part to the optical depth of CS, the  $\text{C}^{18}\text{O}$  is optically thin in this region (see § 5.2.2). Figure 6 shows that the CS has a much broader distribution on the sky compared to the  $\text{N}_2\text{H}^+$  despite the similarity in critical density values for the transitions. A depression in the CS emission  $\sim 1'$  northwest of the peak  $\text{N}_2\text{H}^+$  and  $\text{NH}_3$  emission is also seen in Figure 6 that coincides with a deficit in  $\text{C}^{18}\text{O}$  emission. This slight depression is bordered on the southwestern edge by the  $\text{C}_2\text{S}$  emission and may signify a depletion zone.

It is not clear whether or not significant depletion has occurred in the inner regions of L1551 MC since chemical effects cannot be sufficiently isolated with our models. How-

ever, the relative deficit of emission from both C<sup>18</sup>O and CS at small radii indicate some depletion of these species has occurred presumably due to chemical evolution related to core contraction (e.g. Lee et al. 2004).

### 5.2.2. CO Isotopologue Emission

Figure 3 shows the best fit to the composite CO isotopologue spectra and Table 5 outlines the fit results. The best fit turbulent velocities for our CO isotopologues are a factor of 1.5 higher than the CS and N<sub>2</sub>H<sup>+</sup> fits. These larger values are likely due to the CO isotopologues tracing a larger volume along the line of sight. The CO isotopologues are tracing cold gas with the <sup>13</sup>CO and C<sup>18</sup>O being optically thick and thin respectively.

The abundance of both isotopologues derived from our models are consistent with observations (e.g., Frerking et al. 1982; Lada et al. 1994) given the stated uncertainties. The best fits for  $X_{^{13}\text{CO}}$  and  $X_{\text{C}^{18}\text{O}}$  are  $1.1 \times 10^{-6}$  and  $1.1 \times 10^{-7}$  respectively. For all our models the ratio of these abundances most consistent with the observed CO isotopologue line intensities is  $\approx 10$ ; a factor of 2 higher than what would be estimated from terrestrial abundance ratios (Pickett et al. 1998).

The centroid of the C<sup>18</sup>O line agrees well with the centroid of the N<sub>2</sub>H<sup>+</sup> (see Figure 3) in accord with the results from Lee et al. (2001). The shape of the <sup>13</sup>CO line profile, slightly broadened by optical depth, is fit well with model A-II, but the central velocity is clearly shifted. This shift accounts for the anomalously high RMSE values in Table 5. A cross correlation between the model A-II fit and the observed spectrum peaks at a lag of 7.1 kHz corresponding to a velocity offset of 0.02 km s<sup>-1</sup> at this transition frequency. This is not accounted for in the stated measurement errors for the published frequency equal to 5.1 kHz (Pickett et al. 1998). If this offset were due to an error in the chosen observing frequency, a best estimate of the true frequency would be 110.2013470 GHz.

### 5.3. Is the C<sub>2</sub>S Emission Tracing the CS Self-Absorbing Gas?

It is likely that CS and C<sub>2</sub>S share the same chemical pathway in the interstellar medium (e.g., Suzuki et al. 1992). Yet the critical density of CS(2 – 1) is an order of magnitude higher than C<sub>2</sub>S(3<sub>2</sub> → 2<sub>1</sub>) (Wolkovitch et al. 1997). It is therefore possible for these species to exist in the same environment in different excitation states. The C<sub>2</sub>S emission in L1551 MC is shifted to the red of the systemic velocity (see Paper I) while the CS spectrum shows redshifted self-absorption.

Figure 7 shows composite spectra of the CS and C<sub>2</sub>S lines averaged within a half maximum power contour of the C<sub>2</sub>S emission (see Figure 6). The composite CS spectrum shows a blue peaked, asymmetric profile. The best fit to this spectrum using the HILL5 model returns an infall velocity of 0.14 km s<sup>-1</sup>, nearly identical to the velocity centroid of the C<sub>2</sub>S emission.

This supports the idea that the C<sub>2</sub>S emission is tracing the CS absorption layer, but it still remains unclear why there is no blue component to the C<sub>2</sub>S profile. Chemistry is likely responsible.

## 6. Conclusions

High spectral resolution maps of CS and N<sub>2</sub>H<sup>+</sup> taken with the FCRAO 14 m telescope are fit with two distinctly different radiative transfer models to gain insight into the dynamical and chemical evolution of the recently discovered PPC in Taurus, L1551 MC.

The analytic and numerical models both suggest that L1551 MC is in the early stages of dynamical evolution. Infall velocities of  $\gtrsim 0.1$  km s<sup>-1</sup> are needed in the outer regions of L1551 MC to fit our data adequately. This translates to an accretion rate of  $\sim 10^{-6} M_{\odot}$  yr<sup>-1</sup>, uncertain to within a factor of 5. The observed dynamics are not due to gravitational collapse and are not consistent with the standard picture for low mass star formation. The extent and shape of the asymmetric CS line profiles are more consistent with planar accretion.

There is modest evidence for chemical depletion near the highest density regions of L1551 MC in CS and C<sup>18</sup>O. This suggests that L1551 MC is chemically young. Our models are not very sensitive to chemical evolution and do not shed light on this issue.

Fits to our CO isotopologue data yield a <sup>13</sup>CO to C<sup>18</sup>O relative abundance ratio of  $\approx 10$ . These fits also reveal the <sup>13</sup>CO line centroid to be shifted relative to the other molecular species by 7.1 kHz or 0.02 km s<sup>-1</sup>. If this is due to an incorrect observing frequency, the best estimate for the true transition frequency is 110.2013470 GHz.

The C<sub>2</sub>S emission seen in Paper I may be tracing the infalling CS gas that is producing the observed self-absorption. This would explain the apparent velocity offset of C<sub>2</sub>S with respect to the optically thin, high density tracers. However, it is unclear why there is no blue component to the C<sub>2</sub>S line profile.

The gas dynamics and distributions of molecular species in L1551 MC are distinct from the complex processes related to the known young stellar objects within the greater L1551 region and are evidence for continued star formation in this evolved cloud.

Thanks to Mark Heyer for help with the data collection and reduction. J. S. would also like to thank P. C. Myers for an enlightening discussion and H. Dickel for the “RT” code and correspondence throughout. We thank Al Glassgold for insightful suggestions. This research was partially supported by the National Science Foundation under grant AST 02-28963.

Facilities: FCRAO 14 m Telescope

## REFERENCES

- Aikawa, Y., Herbst, E., Roberts, H. & Caselli, P. 2005, *ApJ*, 620, 330.
- Ciolek, G. E. & Mouschovias, T. Ch. 1995, *ApJ*, 454, 194.
- Bergin, E. & Langer, W. 1997, *ApJ*, 486, 316.
- Caselli, P., Walmsley, C. M., Tafalla, M., Dore, L. & Myers, P. C. 1999, *ApJ*, 523, 165.
- De Vries, C. H. & Myers, P. C. 2005, *ApJ*, 620, 800.
- Devine, D., Reipurth, B. & Bally, J. 1999, *AJ*, 118, 972.
- Dickel, H. R. & Auer, L. H. 1994, *ApJ*, 437, 222.
- Evans, N. 1999, *ARA&A*, 37, 311.
- Fatuzzo, M., Adams, F. C. & Myers, P. C. 2004, *ApJ*, 615, 813.
- Frerking, M. A., Langer, W. D. & Wilson, R. W. 1982, *ApJ*, 262, 590.
- Kuiper, T., Langer, W. & Velusamy, T. 1996, *ApJ*, 468, 761.
- Lada, C. J., Lada, E. A., Clemens, T. P. & Bally, J. 1994, *ApJ*, 429, 694.
- Lee, J.-E., Bergin, E. A. & Evans, N. J. 2004, *ApJ*, 617, 360.
- Lee, J.-E., Evans, N. J., Shirley, Y. L. & Tatematsu, K. 2003, *ApJ*, 583, 789.
- Lee, C. W., Myers, P. C. & Tafalla, M. 1999, *ApJ*, 526, 788.
- Mardones, D., Myers, P. C., Tafalla, M., Wilner, D. J., Bachiller, R. & Garay, G. 1997, *ApJ*, 489, 719.
- Moriarty-Schieven, G. H. & Snell, R. L. 1988, *ApJ*, 332, 364.

- Moriarty-Schieven, G. H. & Wannier, P. G. 1991, *ApJ*, 373, 23.
- Moriarty-Schieven, G., Butner, H. & Wannier, P. 1995, *ApJ*, 445, L55.
- Myers, P., Mardones, D., Tafalla, M., Williams, J., Wilner, D. 1996, *ApJ*, 465, L133.
- Myers, P. C. 2005, *ApJ*, 623, 280.
- Pickett, H., Poynter, R., Cohen, E., Delitsky, M., Pearson, J. & Muller, H. 1998, *J. Quant. Spec. Radiat. Transf.*, 60, 883.
- Pound, M. W. & Bally, J. 1991, *ApJ*, 383, 705.
- Rawlings, J. M. C., Hartquist, T. W., Menten, K. M. & Williams, D. A. 1992, *MNRAS*, 255, 471.
- Rawlings, J. M. C. & Yates, J. A. 2001, *MNRAS*, 326, 1423.
- Schieven, G. H. 2004, private communication.
- Shu, F. H. 1977, *ApJ*, 214, 488.
- Shu, F., Adams, F. & Lizano, S. 1987, *ARA&A*, 25, 23.
- Snell, R., Loren, R. & Plambeck, R., 1980, *ApJ*, 239, 17.
- Snell, R. 1981, *ApJS*, 45, 121.
- Suzuki, H., Yamamoto, S., Ohishi, M., Kaifu, N., Ishikawa, S., Hirahara, Y. & Takano, S. 1992, *ApJ*, 392, 551.
- Swift, J., Welch, W. & Di Francesco, J. 2005, *ApJ*, 620, 823 (Paper I).
- Tafalla, M., Mardones, D., Myers, P. C., Caselli, P., Bachiller, R. & Benson, P. J. 1998, *ApJ*, 504, 900.
- Tafalla, M., Myers, P., Caselli, P., Walmsley, C. & Comito, C. 2002, *ApJ*, 569, 815.
- Tafalla, M., Myers, P., Caselli & P., Walmsley, C. 2004, *A&A*, 416, 191.
- Vrba, F., Strom, S & Strom, K. 1976, *AJ*, 81, 958.
- Watson, D. M. & Salpeter, E. E. 1972, *ApJ*, 175, 659.
- Welch, W. J., Hartmann, L., Helfer, T. & Briceño, C. 2000, *ApJ*, 540, 362.

Willacy, K., Langer, W. & Velusamy, T. 1998, *ApJ*, 507, 171.

Williams, J. A., Dickel, H. R. & Auer, L. H. 2004, *ApJS*, 153, 463.

Wolkovitch, D., Langer, W., Goldsmith, P. & Heyer, M. 1997, *ApJ*, 477, 241.

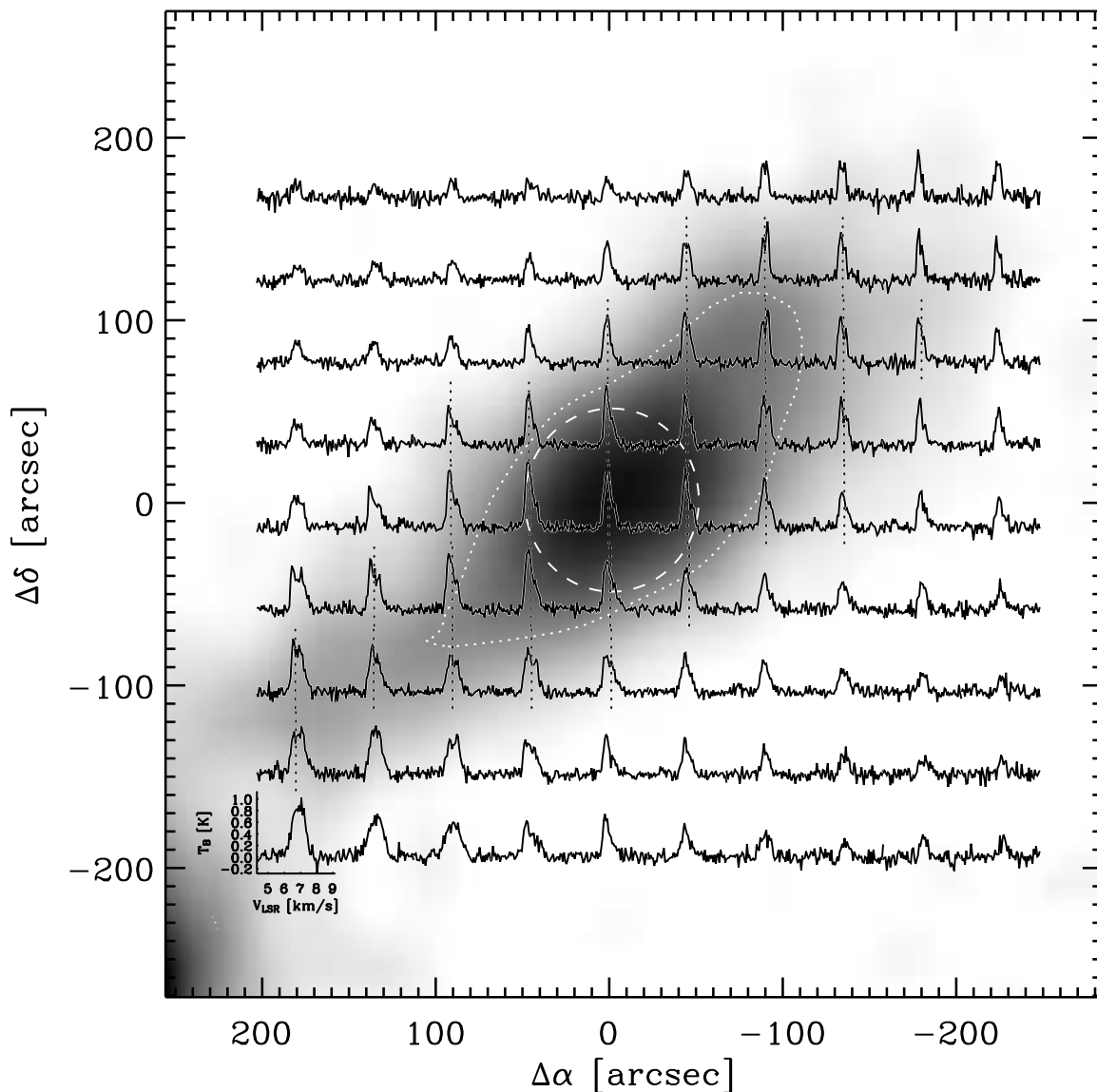


Fig. 1.— Velocity integrated  $\text{N}_2\text{H}^+$  emission from L1551 MC in greyscale with independent spectra of  $\text{CS}(2-1)$  overlaid at their respective positions. The dotted contour represents the 50% peak  $\text{N}_2\text{H}^+$  emission contour. The dashed circle denotes the region in which composite spectra were constructed for  $\text{N}_2\text{H}^+$ , CS,  $^{13}\text{CO}$ , and  $\text{C}^{18}\text{O}$ . The vertical dotted lines in selected spectra represent the systemic velocity along the line-of-sight determined from fits to the  $\text{N}_2\text{H}^+$  spectra at the respective locations.



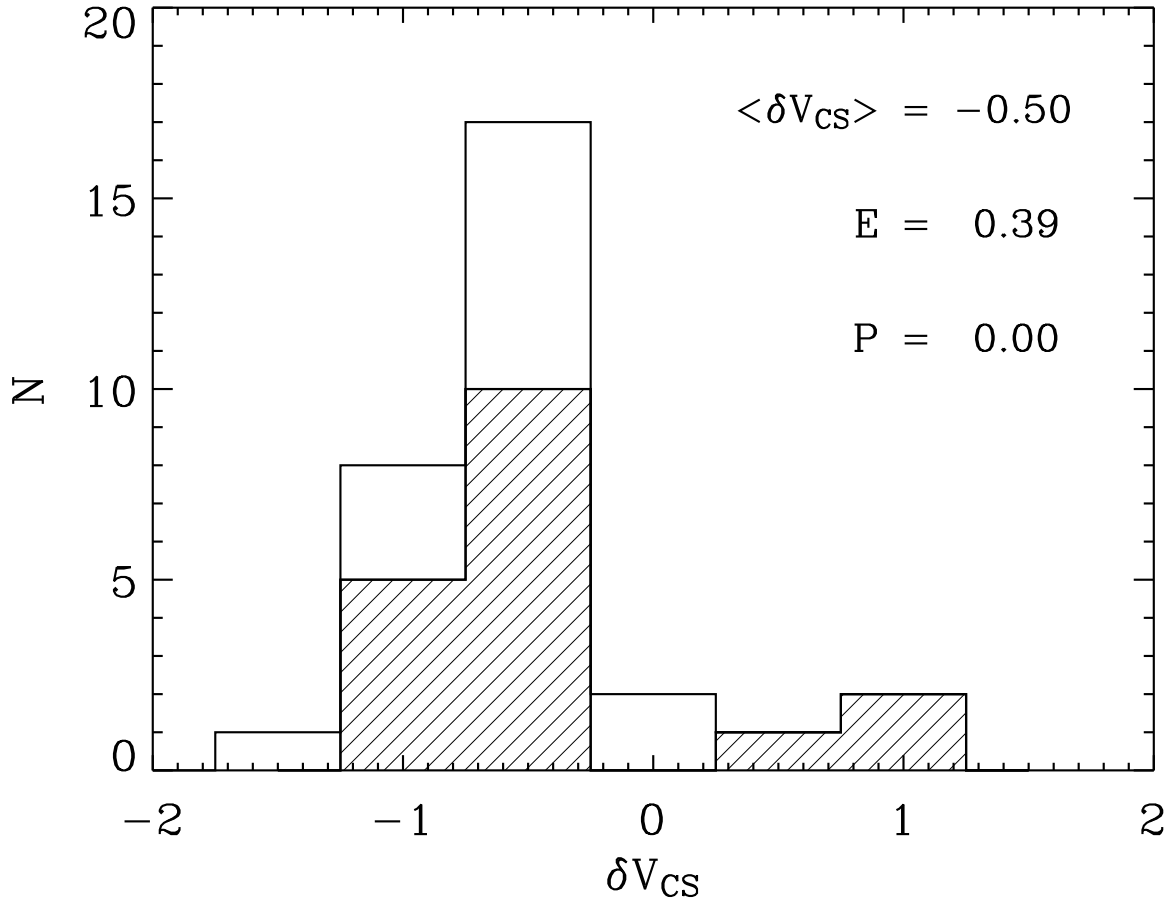


Fig. 2.— Histogram of  $\delta V_{CS}$  values for all spectra with reliable velocity centroids determined from fits to the  $N_2H^+$  data. The shaded region corresponds to the histogram of spectra with  $|\delta V_{CS}| \geq 5\sigma_\delta$ . See § 4.1 for details.

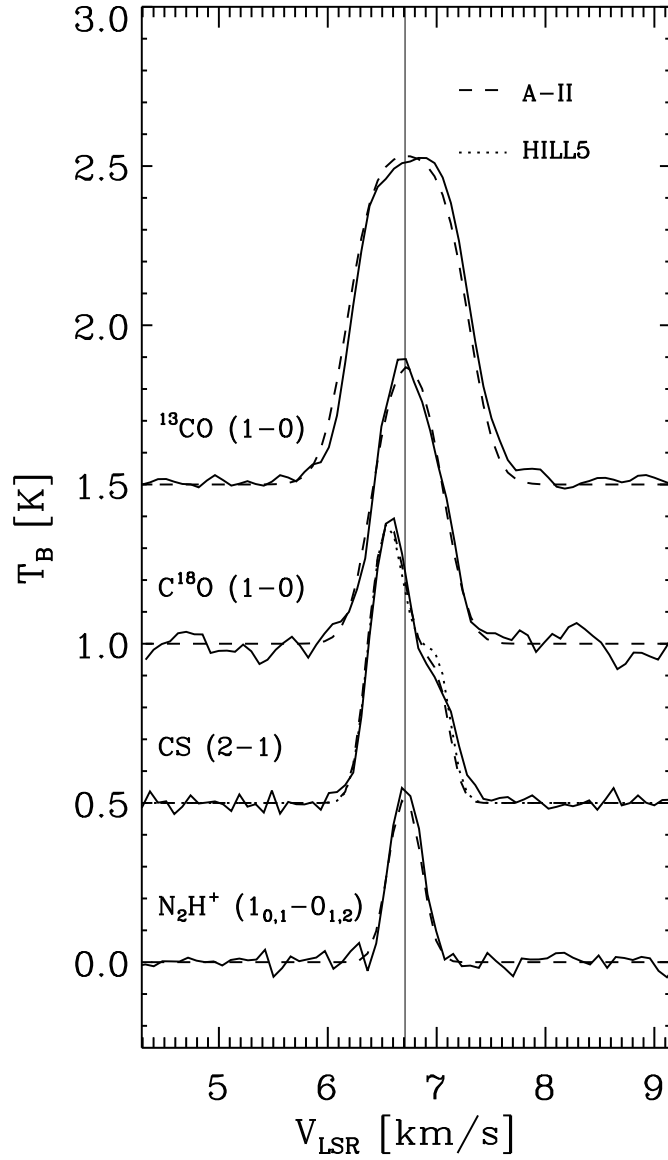


Fig. 3.—  $\text{N}_2\text{H}^+$ , CS,  $\text{C}^{18}\text{O}$ , and  $^{13}\text{CO}$  composite spectra in brightness temperature units. The scale of the  $\text{C}^{18}\text{O}$  and  $^{13}\text{CO}$  spectra are reduced by a factor of 2 and 5 respectively. The model A-II fits to all spectra and HILL5 fit to the CS spectrum are shown as dashed and dotted lines respectively. The thin vertical line signifies the velocity centroid of the  $\text{N}_2\text{H}^+$  line.

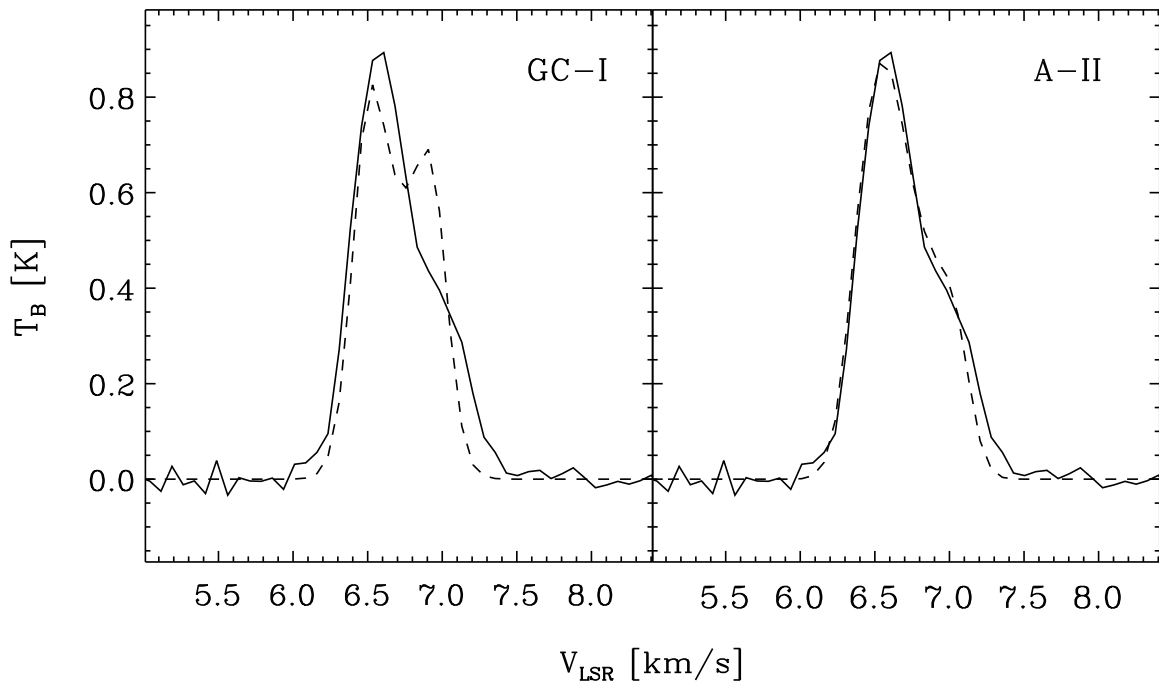


Fig. 4.— Comparison between the best fit “collapse” model, GC-I, to the best fit “accretion” model, A-II. The solid line denotes the data while the model fits are represented with the broken line. See §5.1.1 for details.

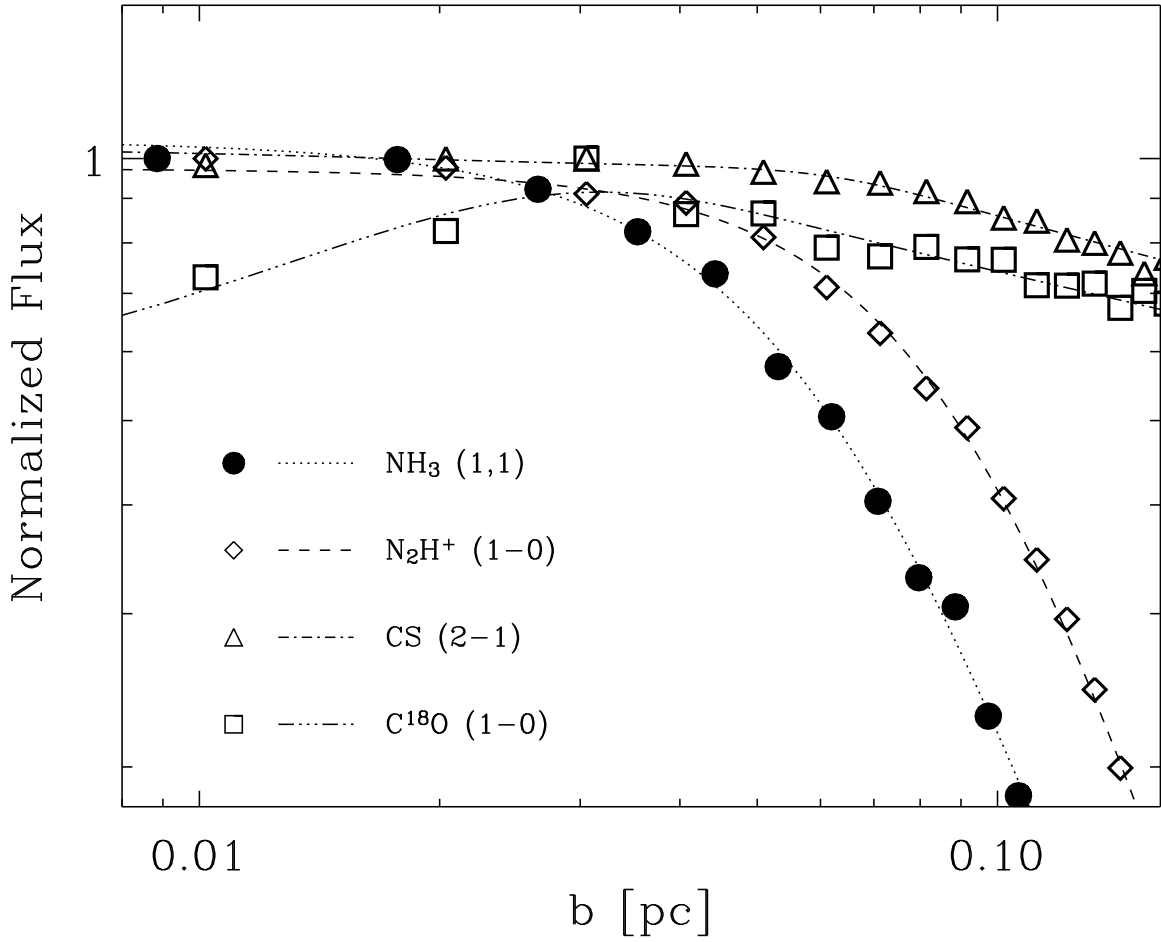


Fig. 5.— Profiles of four different molecular species averaged in elliptical annuli around L1551 MC. For each species the flux is normalized to the peak value in the profile. Equation 1 (for  $\text{NH}_3$  and  $\text{N}_2\text{H}^+$ ) and Equation 2 (for  $\text{CS}$  and  $\text{C}^{18}\text{O}$ ) from Paper I are used to fit the profiles.

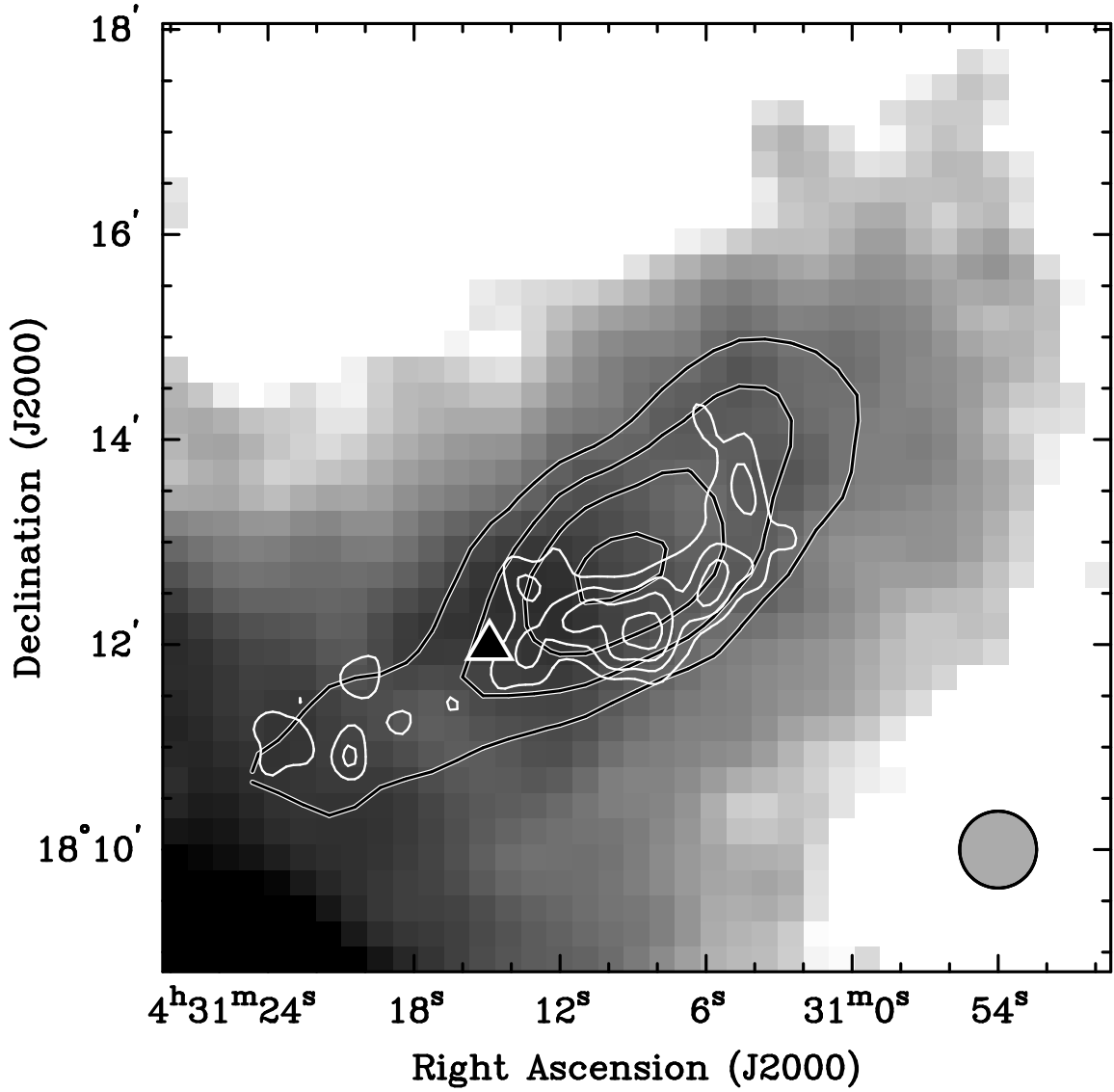


Fig. 6.— Velocity integrated CS in greyscale overlaid with contours of  $\text{N}_2\text{H}^+$  (black contours) and  $\text{C}_2\text{S}$  (white contours; Paper I) at 30, 50 70 and 90% peak flux. The beam size for the CS and  $\text{N}_2\text{H}^+$  data is shown at the bottom right. The black triangle denotes the position of HH265.

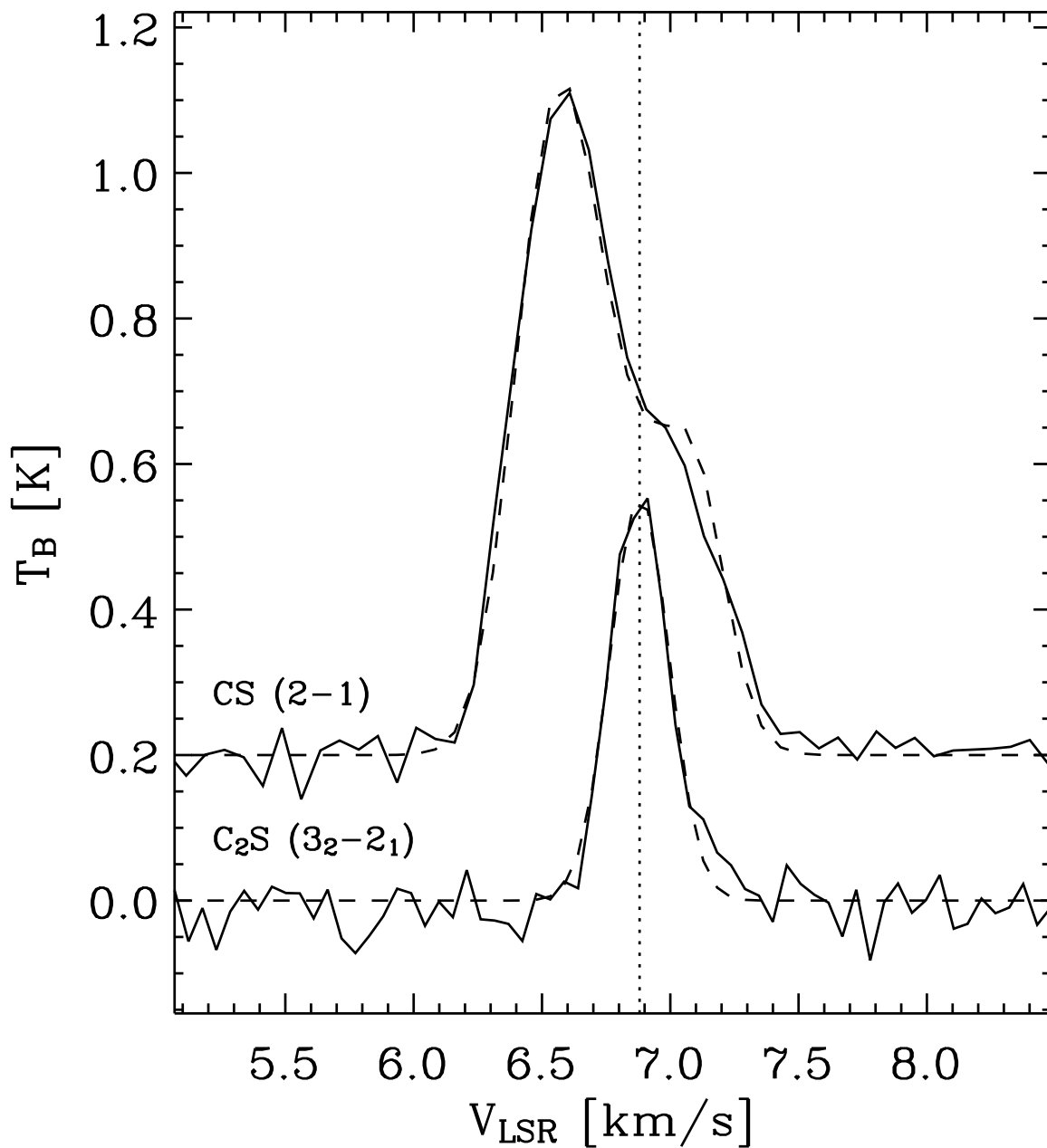


Fig. 7.— CS and C<sub>2</sub>S spectra averaged over the half maximum contour of C<sub>2</sub>S emission in L1551 MC. The vertical dotted line shows the central velocity of the infalling layer determined from the HILL5 fit to the CS line profile and is seen to be nearly identical to the velocity centroid of the C<sub>2</sub>S line profile fit by a single Gaussian component.

Table 1. Overview of Numerical Cloud Models

Model Parameter	Value
$n(r)$ .....	$n_0/[1 + (r/r_c)^\alpha]$ $\text{cm}^{-3}$
$n_{mol}(r)$ .....	$X_{mol}(r)^\dagger n(r)$ $\text{cm}^{-3}$
$v(r)$ .....	$v_0 (r/r_{min})^p$ $\text{km s}^{-1}$
$\Delta v_{turb}$ .....	$0.2 \text{ km s}^{-1}$
$T_K$ .....	9 K
$r_{min}$ .....	67 AU
$r_{max}$ .....	0.2 pc
$r_c$ .....	0.05 pc
$\alpha$ .....	2.2

$^\dagger X_{mol}(r)$  is either constant with radius or takes the form of Equation 2.

Table 2. Family of Numerical Models

Model Name	Velocity Profile	Abundance Profile	Comments
“Accretion” Models			
ACV-I	$v(r) = \text{constant}$	$X_{mol}(r) = \text{constant}$	Numerical analogue to HILL5 model.
ACV-II	$v(r) = \text{constant}$	$X_{mol}(r) = \text{“drop”}^a$	Like model ACV-I but with central depletion.
A-I	$v(r) \propto r^{1/2}$	$X_{mol}(r) = \text{constant}$	High velocity gas at large core radii.
A-II	$v(r) \propto r^{1/2}$	$X_{mol}(r) = \text{“drop”}^a$	Like model A-I but with central depletion.
“Collapse” Models			
GC-I	$v(r) \propto r^{-1/2}$	$X_{mol}(r) = \text{constant}$	Inside-out collapse model with constant abundance fraction.
GC-II	$v(r) \propto r^{-1/2}$	$X_{mol}(r) = \text{“drop”}^a$	Inside-out collapse model with central depletion.

<sup>a</sup>See Equation 2.



Table 3. HILL5 Model Fit to Average CS Spectrum

Model Parameter	Best Fit Value
$\tau_C$ .....	2.02
$\sigma$ .....	0.15 km s <sup>-1</sup>
$T_C$ .....	4.57 K
$v_{LSR}$ .....	6.72 km s <sup>-1</sup>
$v_{in}$ .....	0.15 km s <sup>-1</sup>
RMSE <sup>a</sup> .....	2.03

<sup>a</sup>The root mean square of the error as defined in Equation 1.

Table 4. Numerical Model Fits to CS Emission

Name	$n_0$ $10^4 \text{ cm}^{-3}$	$v_0$ $\text{km s}^{-1}$	$X_{CS}$ $10^{-9}$	$\tau_{max}$	RMSE <sup>a</sup>
“Accretion” Models					
ACV-I	4.6	0.16	0.8	2.8	0.95
ACV-II	7.9	0.15	1.1	5.1	1.09
A-I	3.3	0.015	1.4	3.0	0.89
A-II	6.9	0.001	1.4	5.2	0.77
“Collapse” Models					
GC-I	4.2	0.5	1.1	5.1	2.38
GC-II	6.3	0.5	2.1	8.9	2.68

<sup>a</sup>The root mean square of the error as defined in Equation 1.

Table 5. Numerical Model Fits to CO Isotopologue Emission

<sup>13</sup> CO					
Name	$X_{mol}$	$\Delta v_{turb}$ [km s <sup>-1</sup> ]	$T_k$ [K]	$\tau_{max}$	RMSE <sup>a</sup>
ACV-I	6.6(-7)	0.39	8.8	3.1	4.19
ACV-II	9.8(-7)	0.39	8.7	4.9	4.11
A-I	8.6(-7)	0.37	9.0	2.7	4.47
A-II	1.1(-6)	0.38	8.8	4.7	4.18
GC-I	7.9(-7)	0.42	8.7	3.6	3.96
GC-II	1.3(-6)	0.43	8.7	5.2	3.96
<sup>18</sup> O					
ACV-I	6.9(-8)	0.29	9.0	0.37	0.96
ACV-II	1.0(-7)	0.30	9.2	0.58	0.95
A-I	9.2(-8)	0.24	10.3	0.28	1.02
A-II	1.1(-7)	0.28	12.0	0.37	0.99
GC-I	1.0(-7)	0.34	6.1	0.97	0.94
GC-II	1.7(-7)	0.35	6.1	1.4	0.94

<sup>a</sup>The root mean square of the error as defined in Equation 1.